Soft Matter

Cite this: DOI: 10.1039/c2sm07229g

www.rsc.org/softmatter

PAPER

Motion induced by asymmetric enzymatic degradation of hydrogels†

Jennifer H. Hou[a] and Adam E. Cohen*[ab]

Received 21st November 2011, Accepted 21st February 2012
DOI: 10.1039/c2sm07229g

Biological hydrogels are continuously turned over through secretion and degradation. This non-equilibrium flux may be important for cellular and molecular transport through mucus and the extracellular matrix. Gel-digesting enzymes can drastically change the physical and chemical properties of the hydrogel environment. We report that a spatial gradient in the degradation of two gel/enzyme systems—gelatin/trypsin and hyaluronan/hyaluronidase—leads to directional motion of particles embedded in the gel in the direction of higher enzyme concentration. We study the rate at which the degradation front propagates through the gel and the ensuing velocity of the embedded particles, as functions of enzyme and gel concentrations. We propose that asymmetric degradation leads to asymmetric swelling, which transports particles up the enzyme concentration gradient.

1. Introduction

Polymer-based hydrogels are ubiquitous in life—from mucus that lines most internal epithelia of the human body,[1] to the extracellular matrix (ECM) that fills the space between cells,[2] to the extracellular polymeric substance (EPS) secreted by biofilm-forming bacteria.[3] In each case, transport through the hydrogel is critical to the survival of the organism(s). Mucus, in addition to serving as a lubricant, blocks pathogens while passing nutrients, oxygen, or sperm, depending on the organ.[1,4,5] The ECM provides structural support to tissues and organs,[6,7] but also regulates cell-to-cell communication by mechanical and chemical signals.[8,9] Additionally, the ECM serves as a highway for cellular movement, such as keratinocyte migration during wound healing[10] and tumor cell invasion during metastasis.[11,12] EPS anchors bacteria to a favorable surface,[2,3] but also modulates nutrient flow within the bacterial biofilm.[13]

Transport of molecules and cells is sensitive to the physical and chemical properties of the hydrogel environment, which, in turn, are often sensitive to external parameters such as humidity, temperature, pH, and ionic strength. Some cells regulate transport by varying these physical parameters. For example, *Helicobacter pylori*, a bacterium known for its unique ability to colonize the stomach lining and create ulcers, secretes the enzyme urease which raises the pH and thereby lowers the viscosity of gastric mucus.[14] The decrease in viscosity is believed to facilitate colonization by the bacterium.

Many cells and viruses secrete or decorate their surface with gel-degrading enzymes: pathogenic *E. coli*[15] and *Vibrio cholera*[16,17] secrete proteases; influenza decorates its coat with neuraminidase, a glycosidase;[18,19] and metastatic tumors secrete matrix metalloproteases.[11,12] Enzymatic degradation can lead to steep spatial gradients in gel properties, as the enzyme irreversibly cleaves strands of the gel. In turn, spatially heterogeneous changes of the gel parameters can lead to nonequilibrium motion of particles embedded in the gel, *i.e.* the appearance of active transport. Thus it is important to understand how gradients in gel degradation affect the motion of small particles through the gel.

We studied motion of beads embedded in gelatin, in a gradient of trypsin concentration. Trypsin is a serine protease that readily degrades gelatin and is found in the digestive tracts of many vertebrates. We discovered that as the enzyme digested the gel, the beads moved up the enzyme concentration gradient, in the direction of greater gel degradation. We sought a physical model that would explain the existence and direction of this motion, the time of initial bead motion, and the velocity with which the beads first moved. To constrain the model, we simultaneously tracked the motion of the enzyme, the gel, and the beads. We found that enzymatic degradation caused the gel to swell in the direction of maximal degradation. The swelling gel carried the beads with it. This finding suggests that degradation-induced swelling is a possible transport mechanism in nonequilibrium biogels.

2. Results and discussion

2.1. Directed motion of beads in a gradient of enzymatic degradation

We developed a split channel flow cell assay to generate a gradient in trypsin concentration inside a sample of bead-laden gelatin (Fig. 1A). The gelatin was labeled with a blue

[a]*Department of Physics, Harvard University, Cambridge, Massachusetts 02138, USA. E-mail: cohen@chemistry.harvard.edu*
[b]*Department of Chemistry and Chemical Biology, Harvard University, 12 Oxford St, Cambridge, Massachusetts 02138, USA*
† Electronic supplementary information (ESI) available. See DOI: 10.1039/c2sm07229g

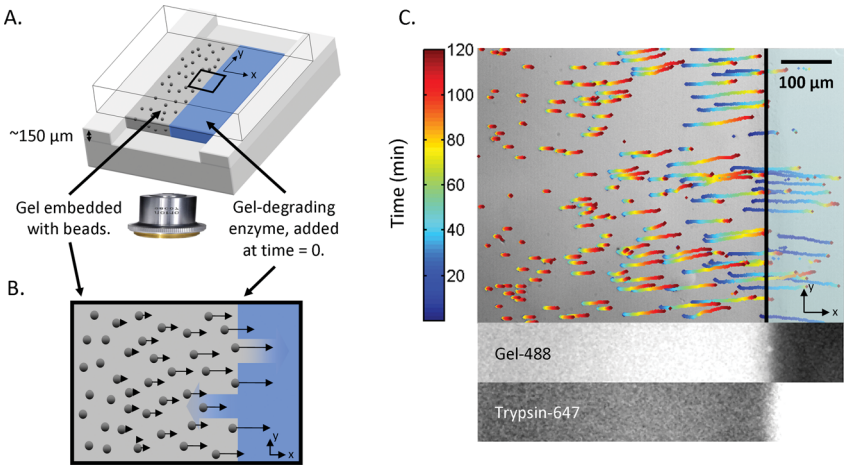

Fig. 1 Particle motion driven by gel swelling under a gradient of enzyme degradation. (A) Experimental setup with split channel flow cell. Half of the flow cell was filled with bead-laden gel. At time = 0, the other half was filled with a gel-degrading enzyme. (B) Microscopic depiction of boxed area in (A). The enzyme (blue) diffused into the gel matrix and degraded the gel. The enzymatic degradation of the gel induced directional motion of both the gel molecules as well as the embedded beads. Beads closer to the interface moved earlier than beads farther from the interface. (C) Time-colored trajectories of beads in a gel degradation gradient overlaid on a brightfield image (top), with simultaneous fluorescence imaging of gelatin-488 (middle) and trypsin-647 (bottom). The black vertical line marks the gel-enzyme interface. The sample is 6 µm polystyrene beads embedded in 5% (w/w) gelatin (left of the interface) with 1 mg mL^{-1} trypsin in 5% digested gelatin (right of the interface). The images were acquired at 12 frames per minute.

fluorophore, Alexa 488 (AF488), and the enzyme was labeled with a red fluorophore, Alexa 647 (AF647), while the beads were visible *via* bright-field microscopy. We used multi-wavelength time-lapse imaging to follow the motion of all three components.

At the start of each experiment, a solution of trypsin in pre-digested gelatin was introduced along one edge of the gelatin. The trypsin diffused into the gelatin, and established an enzyme concentration gradient. This enzyme gradient led to a degradation gradient in the gelatin. The microscopic beads embedded in the gelatin spontaneously moved up the enzyme gradient (Fig. 1B). Digested gelatin also drifted up the enzyme gradient. Control solutions of buffer with no enzyme, or with heat-inactivated enzyme, did not induce bead motion.

Fig. 1C and Supplementary Movie 1 (ESI†) show typical data in which beads, gel, and enzyme were tracked simultaneously. The motion of all three components was predominantly along the x-coordinate (perpendicular to the gel-enzyme interface), and independent of y-coordinate (parallel to the gel-enzyme interface). Thus bead motion, enzyme concentration, and gel concentration were averaged over y and analyzed as functions of x and t (Fig. 2).

The beads underwent three phases of behavior. Initially, the beads were at rest in the gel. As the enzyme permeated and digested the gel, the beads moved toward the interface. Beads closest to the interface moved earliest and fastest, while beads further from the interface moved later and slower. At 5% gelatin, and 1 mg mL^{-1} trypsin, early-moving beads had initial velocities of ~0.2 µm s^{-1} while late-moving beads had initial velocities asymptotically approaching 0.03 µm s^{-1} at $x = -1$ mm from the initial interface (Fig. 2B). Finally, the beads slowed and drifted up the enzyme gradient at ~0.02 µm s^{-1} and began to show detectable Brownian motion, indicating a transition of the gelatin from a gel to a liquid. We call the (x, t)-coordinate at initial bead motion the 'invasion front,' indicated by the grey dotted line in Fig. 2A.

2.2. Motion of beads in homogeneous enzymatic degradation

The experiments in Sec. 2.1 generated gradients in enzyme concentration due to enzyme diffusion, gradients in gel structure due to heterogeneous degradation, and gradients in hydrostatic pressure due to osmotic swelling of the degraded gel. To determine which gradients were responsible for bead motion, we

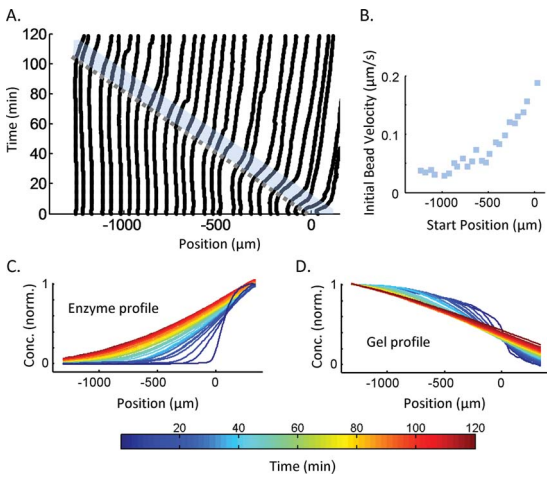

Fig. 2 Transport in an enzymatic degradation gradient. (A) Trajectories of beads as a function of position from interface and time for 5% gelatin and 1 mg mL^{-1} trypsin. Trajectories were acquired from time-lapse images of beads at 12 frames per minute. Net bead motion was toward the gel-enzyme interface, located at $x = 0$. The grey dotted line indicates the 'invasion front', the (x,t)-coordinate at which beads started to move. (B) Initial bead velocities (blue region on A) as a function of starting position for the same data set (5% gelatin and 1 mg mL^{-1} trypsin). Brownian motion of the beads became detectable ~10 min after initial bead movement, coincident with a decrease in bead velocity. (C) Enzyme and (D) gel profiles as a function of position from the interface (x-axis) and time (color).

studied motion of beads in gelatin with spatially homogeneous enzyme concentration, and hence homogeneous gel degradation.

We designed a microfluidic chamber to deliver enzyme rapidly throughout the gel at the start of the experiment. The lid of the split channel flow cell used in Sec. 2.1 was replaced with a slide containing microfabricated grooves (Fig. 3A). These grooves enabled rapid introduction of enzyme over the entire top surface of the gel. Diffusion of enzyme from the grooves into the gel took ~2 min, shorter than any other timescales in the experiment.

Initially, most beads remained stationary. At $t = 12$ min, beads throughout the sample moved in the $+x$-direction at a velocity of ~0.3 μm s^{-1}. This motion lasted for ~5 min, and then slowed. Thereafter, we observed Brownian motion of the beads, indicating a transition from a gel to a liquid.

These observations of bead motion in the absence of gradients in enzyme concentration or gel degradation establish that diffusiophoresis is not necessary for degradation-induced motion. Furthermore, the absence of detectable Brownian motion during the directed motion indicates that the beads remained strongly coupled to the viscoelastic gel network. Thus we infer that the motion of the beads was due to degradation-induced swelling of the gel toward the free solution-gel interface. This inference is corroborated by the gel tracking data in the gradient experiments (Fig. 2D), which showed expansion of the gel accompanying motion of the beads.

Under physiological conditions, one rarely has a homogeneous distribution of enzyme that is suddenly activated; typically, enzyme is produced from a source and diffuses into the gel. Additionally, in the homogeneous degradation experiments, the asymmetric boundary conditions (free on one side, fixed on the other) set the direction of motion. In an enzymatic gradient however, it is the gradient that establishes the asymmetry leading to directed motion. Thus we next sought to determine how enzymatic diffusion and reaction kinetics interacted with gel swelling to produce the motions observed in Sec. 2.1.

We divided the process into three stages: (1) enzyme transport through the gel; (2) enzymatic cleavage of the gel strands; and (3) swelling of the gel to a new hydrostatic quasi-equilibrium and

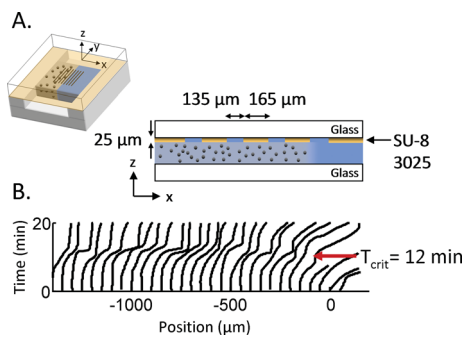

Fig. 3 Particle motion driven by gel swelling under homogeneous enzyme degradation. (A) Experimental setup with split channel flow cell. A micropatterned lid provided vertical confinement while allowing enzyme to permeate the gel homogeneously from the top. The enzyme (blue) quickly diffused vertically into the gelatin, leading to spatially homogeneous degradation. (B) Trajectories of beads as a function of position and time for 5% gelatin and 0.1 mg mL^{-1} trypsin, acquired at 12 frames per minute. At $T_{crit} = 12$ min, the beads synchronously moved toward the free interface.

corresponding motion of the beads. To disentangle the roles of each process on the observed bead motion, we simultaneously tracked the diffusion of the enzyme and the motion of the gel in gradient experiments under different conditions, and also conducted additional experiments on the kinetics of the gel–enzyme reaction in a homogeneous solution.

2.3. Diffusive transport of enzyme through gel

We first analyzed the transport of the enzyme through the gel. The theory of diffusion in gels has been treated previously.[20] A typical profile of enzyme concentration as a function of time is shown in Fig. 2C. To further reduce the dimensionality of the data, we converted each time-dependent concentration profile $\varepsilon(x,t)$ into a dimensionless mean enzyme position $\langle \tilde{x}_{enz}(t) \rangle$, calculated from:

$$\langle \tilde{x}_{enz}(t) \rangle = \frac{\int_0^{x_f} x\varepsilon(x,t)\mathrm{d}x}{x_f \int_0^{x_f} \varepsilon(x,t)\mathrm{d}x}, \quad (1)$$

where x_f is the edge of the gel opposite the initial gelatin-trypsin interface ($x = 0$). Fig. 4A shows $\langle \tilde{x}_{enz}(t) \rangle$ for three gelatin concentrations, all at a trypsin enzyme concentration of 1 mg mL^{-1} (points). The data are well fit by a simple Fickian diffusion model (solid lines, eqn S2, ESI†), with trypsin diffusion coefficients of $D_{tryp} = 42.2$, 44.0, and 29.4 $\mu m^2\ s^{-1}$ in gelatin concentrations 2.5%, 5%, and 10%, respectively. The weak dependence of D_{tryp} on gelatin concentration is consistent with free diffusion of the enzyme through the interstices of the gel, with the enzyme spending little of its time bound to the gel.

To confirm our hypothesis that trypsin diffused almost freely, we compared the diffusion of trypsin in gelatin to the diffusion of free Alexa 647 dye in undegraded gelatin. The dye had larger absolute diffusion coefficients than trypsin, as expected from its smaller molecular size, but showed a similar dependence of D_{dye} on gel concentration. The dye had $D_{dye} = 198$ $\mu m^2\ s^{-1}$ in 5% gel and $D_{dye} = 121$ $\mu m^2\ s^{-1}$ in 10% gel, a 39% decrease, while D_{tryp} decreased by 33% between 5% and 10% gel.

The insensitivity of enzyme diffusion to gel concentration and similarity to free dye diffusion allowed us to rule out significant sticking of the enzyme to the gelatin, significant degradation-dependent modifications in D_{tryp}, and significant changes to enzyme motion due to convection of the buffer or directional motion of the gel.

2.4. Critical enzyme exposure for bead motion

The onset of bead motion in the homogeneous degradation experiments (Sec 2.2) was largely independent of x-position. In contrast, in the gradient experiments (Sec. 2.1), the invasion front propagated through the gel at nearly constant velocity. We define the invasion velocity as the inverse slope of the grey dotted line in Fig. 2A. This velocity increased with enzyme concentration and decreased with gelatin concentration (dark grey bars, Fig. 4C and D). However, the initial bead velocities, averaged over x, were roughly independent of enzyme concentration, and non-monotonic with gelatin concentration, being higher at 5% gel than at 2.5% or 10% (light grey bars, Fig. 4C and 4D).

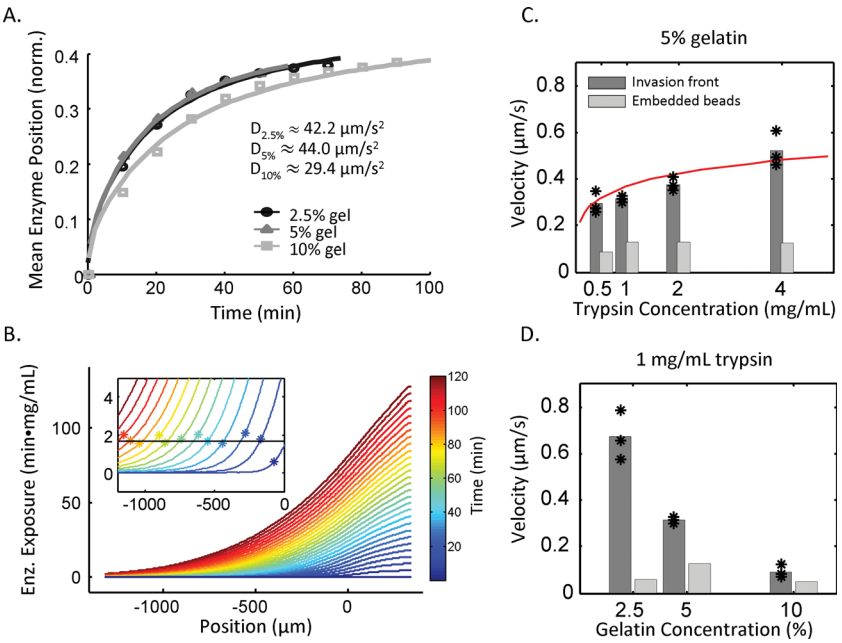

Fig. 4 Characterization of transport as a function of initial enzyme and gel concentrations. (A) The mean penetration of enzyme into the gel as a function of time for three gelatin concentrations. The solid lines are fits to the analytic solution given by eqn S2 (ESI†). Diffusion of the enzyme was only weakly dependent on gelatin concentration. (B) Cumulative enzyme exposure as a function of position and time. (Inset) Zoom-in at low cumulative exposure values. Asterisks indicate the (x,t)-coordinate of the invasion front. The enzyme exposure at these position-time points was constant at 1.6 min mg mL^{-1} (black line). Velocities of invasion front (dark grey bars) and beads (light grey bars) as a function of (C) trypsin concentration at 5% gelatin concentration; (D) gelatin concentration at 1 mg mL^{-1} trypsin concentration. Invasion front bars represent the average of three data sets, whose individual values are indicated by the asterisks. Bead velocity bars represent the mean initial velocities across the three data sets. The red line on (C) is a scaled fit to our model for invasion velocity as a function of enzyme concentration.

We sought a model of the gel degradation process to explain the sudden onset of bead motion (Fig. 2A and 3B), and the dependence of the invasion velocity on enzyme and gel concentrations (Fig. 4C and 4D). Together, these trends suggested that the concentration of gelatin crosslinks, $C(x,t)$, had to pass below a threshold C_{crit} for bead motion to commence.

The enzyme acts as a monomer and the number of enzyme binding sites in the gelatin vastly exceeds the number of enzyme molecules; thus one expects the reaction to be first order in enzyme:

$$\frac{\partial C}{\partial t} \propto \varepsilon, \tag{2}$$

where $C(x,t)$ is the concentration of gel crosslinks and $\varepsilon(x,t)$ is the time-dependent enzyme concentration. This model implies that $C(x,t)$ depends on $\varepsilon(x,t)$ only through the cumulative enzyme exposure, $\mathrm{E}(x,t) = \int_0^t \varepsilon(x,t')\mathrm{d}t'$, regardless of the order of the reaction in C. Thus for each initial enzyme concentration C_0, the critical crosslink concentration for bead motion C_{crit} should correspond to a critical cumulative enzyme exposure, E_{crit}.

The T_{crit} for bead motion in homogeneous degradation conditions corresponds to $\mathrm{E}_{crit} = 1.2$ (min mg mL^{-1}) (Fig. 3B). Similarly, we calculated $\mathrm{E}(x,\ t)$ from the measured $\varepsilon(x,t)$ in gradient degradation conditions for a 5% gel and 1 mg mL^{-1} enzyme source (Fig. 4B). Throughout the gel, bead motion commenced at a characteristic cumulative enzyme exposure $\mathrm{E}_{crit} = 1.6$ (min mg mL^{-1}) (inset, Fig. 4B). The similarities in E_{crit} between the two experiments, and throughout a heterogeneously degraded gel, support the model of a critical crosslink concentration for bead motion.

We combined our finding that enzyme transport was diffusive (Sec. 2.3) with the observation that bead motion commenced at a critical cumulative enzyme exposure to predict the invasion front velocity as a function of initial enzyme concentration. Our simple model captured the dependence of velocity on enzyme concentration observed in our data (red line, Fig. 4C).

We further hypothesized that the gel-enzyme reaction was first order in C, *i.e.*

$$\frac{\partial C}{\partial t} = -k\varepsilon C. \tag{3}$$

Then

$$C(x,t) = C_0 \exp\left(-k\int_0^t \varepsilon(x,t')dt'\right) = C_0 \exp(-k\mathrm{E}(x,t)). \tag{4}$$

We used eqn (4) to predict the motion of the invasion front at several initial gel concentrations. The rate constant k was varied to fit our predictions to the data of Fig. 4D, yielding $k = 0.47$ (min mg mL^{-1})$^{-1}$ at 20 °C.

2.5. Molecular state of gel upon bead motion

We sought to characterize the state of the gel at the onset of bead motion. We quantified the extent of Brownian motion perpendicular to the drift velocity before, during, and after motion.

Before and during bead motion, there were no detectable position fluctuations. After directed motion had slowed, we observed Brownian motion with a diffusion coefficient of $D = 0.05$ $\mu m^2\ s^{-1}$, consistent with a low viscosity liquid. To estimate the magnitude of thermal fluctuations, we calculated the effective spring constant k[21] for displacement of a 6 μm diameter bead in an infinite gel with Young's modulus 40 kPa and Poisson's ratio 0.4, corresponding to the mechanical properties of a 5% gelatin gel.[22–24] From the relation $\langle \delta x^2 \rangle = k_B T/k$, we obtained an amplitude <1 nm, consistent with the absence of detectable thermal fluctuations prior to gel liquefaction.

The bead migration data did not indicate the molecular state of the gelatin at the onset of bead motion. To obtain a more detailed understanding of the process by which trypsin degrades gelatin, we investigated the reaction in bulk solution, where enzyme and gel concentrations were homogeneous in space. We used sodium dodecyl sulfate polyacrylamide gel electrophoresis (SDS-PAGE) to analyze the distribution of gelatin molecular weights as a function of incubation time with enzyme. The degradation products were stained with Coomassie blue (Fig. 5A). At a trypsin concentration of 1 mg mL^{-1}—corresponding to the loading concentration in the bead experiments—the gelatin was degraded into segments smaller than our lower bound of detection (~15 kDa) within one minute of mixing (lane 12 of gel, Fig. 5A). At 300-fold lower trypsin concentration (0.003 mg mL^{-1}), we observed in a span two hours that there was a gradual disappearance of large molecular weight gelatin and appearance of smaller molecular weight fragments. The staining pattern within each lane was converted to a distribution, $\rho(l,t)$, describing the concentration of molecules with molecular weight l at time t (Fig. 5B).

We constructed a microscopic model of gel degradation to explain the measured molecular weight distributions. Trypsin cleaves gelatin at arginine and lysine residues, but only if the residue is not followed by proline.[25] From the amino acid composition of gelatin,[26] we estimated the density of cleavage sites $\alpha \sim 1$ per kDa of gelatin. As a result of the processing from collagen, the molecular weights of gelatin are heterogeneous, ranging from 100–400 kDa. It was thus reasonable to assume that the number of cleavage sites n was proportional to the molecular weight l, so we worked with the distribution $\rho(n,t)$.

Each cleavage event converted a strand with n' cleavage sites into two strands with n and $n' - n - 1$ sites (one site was lost to cleavage). We assumed that after each cleavage event, the enzyme dissociated from the polymer and that there was no correlation between the locations of successive cleavage events. Finally, we assumed that the enzyme had no molecular weight preference, *i.e.* that all cleavage sites were equally good targets, regardless of the length of the chain in which they were embedded. Under these admittedly simplifying assumptions, the evolution of $\rho(n,t)$ is governed by a simple master equation, originally developed in the context of thermal degradation of polymers:[27, 28]

$$\frac{\partial \rho(n,t)}{\partial t} = -\gamma n \rho(n,t) + 2\gamma \sum_{n'=n+1}^{n'=n_{\max}} n' \Omega(n,n') \rho(n',t), \qquad (5)$$

where γ is the rate of scission *per cleavage site* on the polymer backbone. The second term on the right hand side describes the creation of a strand with n sites from one with $n' > n$ sites. The assumption of uniformly distributed random scission implies that

$$\Omega(n,n') = \frac{1}{n'} \text{ for } n < n'. \qquad (6)$$

Using eqn (6), we recast eqn (5) in matrix form:

$$\frac{d\vec{\rho}(t)}{dt} = \gamma \mathbf{T} \vec{\rho}(t), \qquad (7)$$

where

$$\vec{\rho}(t) = \rho(n,t)$$

and the matrix $\mathbf{T}$ is

$$\mathrm{T}_{n,n'} = \begin{cases} 2 & \text{for } n < n' \\ -n & \text{for } n = n' \\ 0 & \text{otherwise} \end{cases}.$$

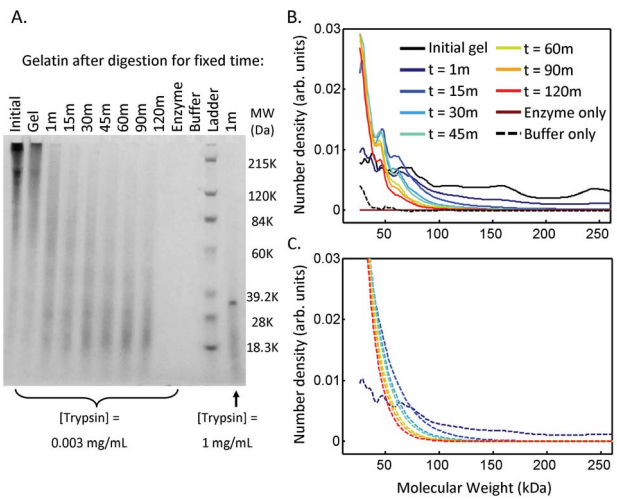

Fig. 5 Degradation of gelatin by trypsin in bulk solution. (A) SDS-PAGE gel of gelatin at enzyme concentrations 0.003 mg mL^{-1} (lanes 2–9) and 1 mg mL^{-1} (lane 12) as a function of incubation time (in minutes). (B) Molecular weight distribution of the gelatin as a function of time. Molecular weight components >100 kDa of the gelatin disappeared within the first minutes of the reaction, and their smaller molecular weight products accumulated over time. (C) Evolution of the molecular weight distribution by a random scission binary fragmentation model, with initial conditions determined by the experimental molecular weight distribution of undegraded gelatin. The model can be matched to data shown in B by assuming a time-dependent rate constant.

We fit eqn (7) to the data in Fig. 5B at $t = 15, 30, 45, 60, 90, 120$ min, using $\vec{\rho}(t = 1\text{min})$ as the initial condition and floating the rate constant γ (Fig. 5C). The good correspondence between the predicted molecular weight distributions (Fig. 5C) and the measured distributions (Fig. 5B) indicates that the simple binary fragmentation model accurately captures the mechanics of the trypsin-gelatin degradation reaction.

The SDS-PAGE data enabled us to determine the degree of gelatin degradation at which beads started to move in the gradient studies. We extrapolated the data in Fig. 5A and B to

the critical cumulative enzyme exposure in the gradient experiments. Bead motion commenced when the gelatin had ~0.13 cuts/kDa and only 1% of the remaining gelatin was larger than 45 kDa. This high degree of degradation prior to bead motion is explained by the fact that the gelatin molecules assemble into higher-order fibrils.[29,30] Cleavage of a single gelatin molecule does not change the crosslink density—only when enzyme has completely cut through a fibril does the crosslink density change.

We compared the cleavage rate γ inferred from bulk degradation with the cleavage rate constant k inferred from the velocity of the invasion front (Sec. 2.4). These rates are related by

$$k = \frac{\gamma\alpha}{[\text{trypsin}]}, \tag{8}$$

where [trypsin] = 0.003 mg mL^{-1} is the concentration in the bulk degradation experiments and $\alpha \sim 1$ cleavage site/kDa gelatin. Using $\gamma \sim 0.002$ cuts/(cleavage site $\times$ min) at time scales of the bead experiments, eqn (8) yields a rate constant $k \sim 0.66$ (min mg mL^{-1})$^{-1}$ at 20 °C. We found in Sec. 2.4 that $k = 0.47$ (min mg mL^{-1})$^{-1}$. The agreement is good, considering the very different types of measurement.

2.6. Mechanism for bead motion

Next we sought to explain how enzymatic degradation led to gel swelling. We propose that enzymatic degradation shifted the equilibrium between osmotic swelling and gel self-attraction. The degree of swelling of a gel is characterized by the volume fraction, $\phi = \frac{V_p}{V_g}$, where V_p is the volume of the dry polymer, and V_g is the volume of the swollen gel. The theory of gel dynamics predicts that in a dilute gel, equilibrium is attained when

$$\phi_{eq} = \chi N_c^{-3/5}, \tag{9}$$

where χ is a material parameter and N_c is the mean number of monomeric segments between crosslinks of the polymer gel.[31] Enzymatic scission of crosslinks caused N_c to increase. Eqn (9) implies that the degradation led to a smaller ϕ_{eq}, and hence to swelling of the gel. Eqn (9) also predicts continuous expansion of the gel as a function of enzyme exposure. We hypothesize that the existence of a critical enzyme exposure prior to expansion was a consequence of the fibrillar nature of the crosslinks: many enzymatic cleavage events were needed before any crosslinks were cut (Fig. 6).

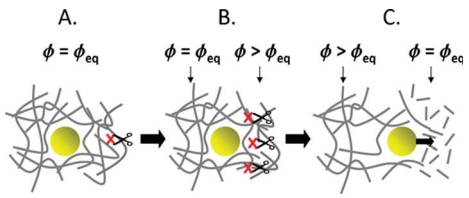

Fig. 6 Mechanism for bead motion. (A) Gelatin starts in equilibrium. Enzyme, represented by scissors, diffuses in the local environment of a bead, but cleavage by enzyme does not change N_c at early times. (B) After a critical threshold of cleavage, N_c changes and shifts the equilibrium volume fraction. (C) As degradation proceeds, the gelatin swells, and pushes the bead forward into the liquefied gel solution.

Was the rate of gel swelling determined by the rate of the enzyme diffusion-reaction, or by hydrodynamic flow into the swelling gel? The approach to hydrostatic equilibrium in a dilute gel is described by Darcy's law

$$v_s - v_p = -\frac{1}{f}\nabla p, \tag{10}$$

where v_s is the velocity of the solvent, v_p is the velocity of the polymer, $f(\phi)$ is the frictional drag per unit gel volume between the polymer and solute, and $p(x, t)$ is the pressure in the gel. Applying incompressibility and mass conservation of the solvent and polymer, Darcy's law leads to a diffusion equation for the pressure:

$$\frac{\partial p(x,t)}{\partial t} = D_s \frac{\partial^2 p(x,t)}{\partial x^2}, \tag{11}$$

where D_s is the ratio of osmotic modulus M to frictional drag f.[31–33] Previous measurements of D_s for gelatin by gel swelling studies *via in situ* interferometry[34] and quasi-elastic light scattering studies[35,36] show that $D_s \sim 20$–40 μm^2 s^{-1}. This estimate, which is on the same order as $D_{tryp} \sim 40$ μm^2 s^{-1} (Sec. 2.3), implies that pressure diffused into the gel on the same time scale as trypsin.

However, we note that our estimate of D_s is only relevant for a solid, undegraded gel. In the gradient experiments, D_s decreased with time due to a degradation-induced decrease in the modulus M. At the end-point of the reaction, the gel was liquid and $M \to 0$, implying that $D_s \to 0$. We propose that due to the high degree of degradation at the onset of gel swelling, D_s was less than D_{tryp} throughout the time of bead motion. Thus the bead velocity was determined by hydrodynamic swelling, independent of bulk enzyme concentration, in agreement with our observations (light grey bars, Fig. 4C).

2.7. Asymmetric degradation of hyaluronan leads to directional motion of embedded beads

To test the generality of degradation-induced motion in gels, we studied the motion of beads in hyaluronan subject to asymmetric degradation by hyaluronidase. Hyaluronan is a large polymer of disaccharides, ranging from 5 kDa to 2×10^4 kDa.[37] As with collagen, hyaluronan is a major component of the ECM and serves as a lubricant and structural barrier.[37] This biogel interacts with cell surface receptors, and is thought to play an important role in the proliferation and migration of cancer cells.[38,39] We prepared split channel flow cells as we had for gelatin: an aqueous gel of hyaluronan, doped with beads, was placed in one half of the channel, and a solution of hyaluronidase was flowed in the other half. As the enzyme degraded the gel, the beads moved toward the degradation front. Initial motion of the beads followed an invasion front, similar to the behavior in gelatin/trypsin (Fig. 7). The degraded hyaluronan had sufficiently low viscosity that the beads settled and stopped moving ~30 min after the initial motion. These observations establish that motion induced by asymmetric gel degradation occurs in both protein and carbohydrate-based biogels.

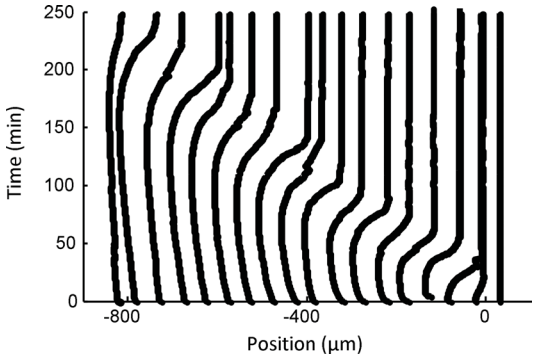

Fig. 7 Degradation-induced motion of beads in a hyaluronan gel (1% w/w) with hyaluronidase (1 mg mL^{-1}). Trajectories were acquired from time-lapse images of beads at 12 frames per minute. Similar motion to that of gelatin/trypsin was observed for this carbohydrate-based gel.

3. Conclusions

We have shown that asymmetric enzymatic degradation induces motion in a biogel *via* asymmetric swelling of the gel. Understanding the conditions under which this motion occurs can lead to new insights on how pathogenic bacteria invade host organisms, how cancer cells move through the extracellular matrix, and how biofilm-forming bacteria move and communicate with each other.

This mechanism of motion is distinct from the well-known diffusiophoretic effects in which concentration gradients in the liquid state lead to osmotic forces directly on a particle.[40–43] Experimental demonstrations of diffusiophoretic "swimmers" have been restricted to simple liquids.[44] The particle velocities we observe are orders of magnitude larger than would be predicted from diffusiophoresis alone and arise through large-scale reconfigurations of a viscoelastic gel.

Chemically powered phoretic motion in complex fluids offers qualitatively new modes of transport, and is likely to be relevant to biological motility. For instance, the bacterium *Listeria monocytogenes* propels itself within a host eukaryotic cell by an actin-based Brownian ratchet: asymmetric polymerization of the host actin by the bacterium produces a comet tail of stiff actin filaments leading to directed propulsion.[45,46] We speculate that microorganisms may use asymmetric degradation of host biogels to induce directed propulsion as well. By investigating possible mechanisms for selective passage of particles through viscoelastic barriers, one may be able to engineer systems to infiltrate these protective systems for targeted drug delivery.

4. Experimental methods

4.1. Gel–enzyme flow cell experiments

Trypsin from porcine pancreas (Sigma Aldrich T7409) was fluorescently labeled by reaction with Alexa 647 SE (Invitrogen A-20106) in a 1 : 1 molar ratio in 0.1 M pH 8.3 sodium bicarbonate, following manufacturer instructions. Excess dye was removed by spin centrifugation (GE PD SpinTrap G-25 28-9180-04).

Gelatin from bovine skin (Sigma-Aldrich G9391) was fluorescently labeled by reaction with Alexa 488 TFP (Invitrogen A-30005) in a 1 dye : 1 lysine ratio in 0.1 M pH 9.0 sodium bicarbonate, following manufacturer instructions. Excess dye was removed by gravity flow column fractionation (GE PD-10 17-0851-01).

All experiments were performed in phosphate-buffer saline, pH 7.4 (PBS). Carboxylated polystyrene beads (6 μm diameter; Phosphorex 117) were washed by centrifugation (3 × 5 min at 15,000 g) to remove residual surfactant, and then re-suspended in PBS. Lyophilized gelatin was hydrated in the washed bead suspension at 2.5%, 5%, or 10% (w/v) and heated at 60 °C until all pellets of gelatin were visibly dissolved. Gelatin-488 was doped into the unmodified bead-gelatin mixture in a 1 : 60 ratio.

To eliminate possible osmotic imbalances due to gelatin degradation products, the enzyme was pre-mixed with gelatin before the experiment. Trypsin-647 was doped into unmodified trypsin solution in a 1 : 90 ratio. The trypsin solution was mixed with unlabeled gelatin for a final trypsin concentration of 0.5, 1, 2, or 4 mg mL^{-1} and final gelatin concentration to match that of the bead-gelatin mixture. The trypsin-gelatin solution was incubated at 4 °C for 3 h, ensuring complete degradation of the gelatin. The mixture remained liquid, as the trypsin digested the gelatin and prevented gelation.

For the gradient studies (Sec. 2.1), microfluidic channels were made with glass slides as the bottom and top surfaces, and sealed with melted parafilm (Fig. 1A). Half the width of the channel was temporarily filled with plastic shim of thickness 150 μm. The pre-heated microfluidic channels were filled with the molten bead-laden gelatin, and the gelatin was allowed to solidify at 4 °C for 3 h at 100% relative humidity. The sample was brought up to room temperature and mounted on the microscope. The plastic spacer was removed, and the empty half of the chamber was filled with the solution of trypsin and degraded gelatin.

For experiments on bead motion in uniformly degrading gelatin (Sec. 2.2), a microfluidic system was used to deliver enzyme homogeneously throughout the gel. Gel was cast in a flow cell similar to that used in Sec. 2.1. The top surface was removed, and replaced with a glass slide patterned with microchannels for trypsin delivery.

The microchannels were made by photolithography using SU-8 3025 (MicroChem). Channels were 1 cm (L) × 135 μm (W) × 25 μm (D), spaced by 165 μm, and covered a 1 cm × 1 cm window. The rest of the glass was coated in a 25 μm layer of SU-8. The slide was baked for 2 h at 150 °C to promote adhesion of the SU-8. The slide was then plasma cleaned for 5 min to render the SU-8 hydrophilic. The dimensions of the channels were chosen based on $D_{tryp} = 44.0\ \mu m^2\ s^{-1}$ in 5% gelatin (Sec. 2.3) to allow trypsin to diffuse homogeneously throughout the sample within ~2 min.

As the enzyme digested the gel at room temperature (20 °C), time-lapse images were acquired on one of two setups: (1) a custom-built inverted microscope with 4× magnification equipped with a QSI 504 camera and wide-field illumination by light emitting diodes (Luxeon V Star LXHL-LB5C) with corresponding filter cube (Olympus U-MWB2) or (2) an inverted Nikon TE-2000e microscope with 4× magnification equipped with a Hamamatsu 1394 ORCA-ERA camera and wide-field illumination by an X-Cite mercury lamp. Enzyme and gel motion were followed by fluorescence, and bead motion by white light *trans*-illumination.

Preparation of sample chambers with hyaluronan (Sigma-Aldrich 53747) and hyaluronidase (Sigma-Aldrich H3884) followed the same procedure as for the gelatin/trypsin experiments.

4.2. Bulk kinetics and SDS-PAGE studies

Solubilized trypsin and molten gelatin were prepared as described in Sec. 4.1, but without beads and fluorescent doping. Gelatin-trypsin samples were incubated at 20 °C on a tube rotator for the prescribed time and then boiled at 100 °C in 0.1 M Tris, 0.1 M HEPES, 3 mM SDS, 75 mM DTT, pH 8 for 5 min. Reaction products were fractionated *via* SDS-PAGE (Thermo Scientific Precise Protein Gels, 4–20%, 25244) at 135 V for 50 min. The gels were visualized with Coomassie Blue R-250 by staining overnight in a solution of 1% Coomassie R-250, 10% acetic acid, and 40% methanol, followed by destaining in 10% acetic acid, 40% methanol for 4–6 h. The SDS-PAGE gel was evenly *trans*-illuminated with a light emitting capacitor (CeeLite) for digital photography. Images were processed in Matlab.

4.3. Data analysis

Movies of bead motion were analyzed as follows. Each image was bandpass filtered with a lower bound of 2 pixels and an upper bound of 10 pixels to remove point defects and to correct for uneven illumination. Features were identified in each movie frame by brightness: only pixels less than three standard deviations of the mean pixel intensity were retained. Remaining features were then further culled by area: only features within two standard deviations of the mean area were kept. The Matlab adaptation[47] of the IDL Particle Tracking Code of Crocker and Grier[48] was used find the centroids of the features, with a peak width of 9 pixels, and then to stitch the lists of centroids together into trajectories. The particles were expected to move at most 9 pixels between tracked frames and were allowed to disappear for at most four frames. Only trajectories that started in the first frame and lasted for more than 25% of the movie were kept. Trajectories of stuck particles were removed by hand.

Fluorescent images of gel-488 and trypsin-647 were corrected for dark counts and uneven illumination by a flat-field reference. Images were median-filtered to remove specks of dirt, and then averaged over the y-dimension to obtain intensity profiles as a function of (x, t).

SDS-PAGE images were analyzed using the reference ladder to map the spatial distribution of Coomassie blue stain of each lane to a number density profile as a function of molecular weight. The lane profiles were background-corrected by subtracting off the intensity profile of the enzyme-only control lane.

Acknowledgements

This work was funded by the Harvard Materials Research Science and Engineering Center (MRSEC) under grant DMR-0820484, a Sloan Foundation Fellowship, and NSF Grant CHE-0910824. We thank Katharina Ribbeck (MIT) and Zhigang Suo (Harvard) for insightful discussions, and the Center of Brain Sciences (Harvard) for use of their microscope facilities. JHH thanks NDSEG and NSF for supporting her graduate studies.

References

1 D. J. Thornton and J. K. Sheehan, *Proc. Am. Thorac. Soc.*, 2004, **1**, 54.
2 E. D. Hay, *Cell biology of extracellular matrix*, Springer, 1991.
3 H. C. Flemming and J. Wingender, *Nature Reviews Microbiology*, 2010, **8**, 623–633.
4 S. Linden, P. Sutton, N. Karlsson, V. Korolik and M. McGuckin, *Mucosal Immunol.*, 2008, **1**, 183–197.
5 R. A. Cone, *Adv. Drug Delivery Rev.*, 2009, **61**, 75–85.
6 F. T. Bosman and I. Stamenkovic, *J. Pathol.*, 2003, **200**, 423–428.
7 G. M. Fomovsky, S. Thomopoulos and J. W. Holmes, *J. Mol. Cell. Cardiol.*, 2010, **48**, 490–496.
8 F. Rosso, A. Giordano, M. Barbarisi and A. Barbarisi, *J. Cell. Physiol.*, 2004, **199**, 174–180.
9 K. Y. Tsang, M. C. H. Cheung, D. Chan and K. S. E. Cheah, *Cell Tissue Res.*, 2010, **339**, 93–110.
10 P. Martin, *Science*, 1997, **276**, 75.
11 F. Sabeh, R. Shimizu-Hirota and S. J. Weiss, *J. Cell Biol.*, 2009, **185**, 11.
12 W. G. Stetler-Stevenson and A. E. Yu, 2001, **11**, pp. 143–153.
13 P. Stoodley, I. Dodds, J. Boyle and H. Lappin-Scott, Seminars in Cancer Biology, *J. Appl. Microbiol.*, 1998, **85**, 19S.
14 J. P. Celli, B. S. Turner, N. H. Afdhal, S. Keates, I. Ghiran, C. P. Kelly, R. H. Ewoldt, G. H. McKinley, P. So, S. Erramilli and R. Bansil, *Proc. Natl. Acad. Sci. U. S. A.*, 2009, **106**, 14321–14326.
15 R. A. Kramer, D. Zandwijken, M. R. Egmond and N. Dekker, *Eur. J. Biochem.*, 2000, **267**, 885–893.
16 M. E. Scott, Z. Y. Dossani and M. Sandkvist, *Proc. Natl. Acad. Sci. U. S. A.*, 2001, **98**, 13978–13983.
17 A. J. Silva, K. Pham and J. A. Benitez, *Microbiology*, 2003, **149**, 1883–1891.
18 M. N. Matrosovich, T. Y. Matrosovich, T. Gray, N. A. Roberts and H. D. Klenk, *J. Virol.*, 2004, **78**, 12665.
19 T. Kuiken, E. C. Holmes, J. McCauley, G. F. Rimmelzwaan, C. S. Williams and B. T. Grenfell, *Science*, 2006, **312**, 394.
20 M. A. Lauffer, *Biophys. J.*, 1961, **1**, 205–213.
21 L. D. Landau and E. M. Lifshitz, *Theory of Elasticity*, Elsevier, New York, 1986.
22 A. Markidou, W. Y. Shih and W. H. Shih, *Rev. Sci. Instrum.*, 2005, **76**, 064302.
23 C. Joly-Duhamel, D. Hellio, A. Ajdari and M. Djabourov, *Langmuir*, 2002, **18**, 7158–7166.
24 M. Djabourov, J. P. Lechaire and F. Gaill, *Biorheology*, 1993, **30**, 191–205.
25 B. Keil, *Specificity of proteolysis*, Springer-Verlag, Berlin; New York, 1992.
26 W. F. Harrington and P. H. Von Hippel, *Adv. Protein Chem.*, 1961, **16**, 1–138.
27 B. J. McCoy and M. Wang, *Chem.Eng. Sci.*, 1994, **49**, 3773–3785.
28 R. Aris and G. Gavalas, *Philos. Trans. R. Soc. London, Ser. A*, 1966, **260**, 351.
29 C. Robinson and M. Bott, *Nature*, 1951, **168**, 325–326.
30 M. Djabourov, J. Leblond and P. Papon, *J. Phys.*, 1988, **49**, 319–332.
31 D. Masao, *J. Phys. Soc. Jpn.*, 2009, **78**, 052001.
32 T. Tanaka and D. J. Fillmore, *J. Chem. Phys.*, 1979, **70**, 1214.
33 Y. Li and T. Tanaka, *J. Chem. Phys.*, 1990, **92**, 1365.
34 C. Wu and C. Y. Yan, *Macromolecules*, 1994, **27**, 4516–4520.
35 E. J. Amis, P. A. Janmey, J. D. Ferry and H. Yu, *Macromolecules*, 1983, **16**, 441–446.
36 T. Herning, M. Djabourov, J. Leblond and G. Takerkart, *Polymer*, 1991, **32**, 3211–3217.
37 T. C. Laurent, U. B. G. Laurent and J. R. E. Fraser, *Immunol. Cell Biol.*, 1996, **74**, A1–A7.
38 K. N. Sugahara, T. Murai, H. Nishinakamura, H. Kawashima, H. Saya and M. Miyasaka, *J. Biol. Chem.*, 2003, **278**, 32259.
39 S. Adamia, C. A. Maxwell and L. M. Pilarski, *Curr. Drug Targets: Cardiovasc. & Haematol. Disord.*, 2005, **5**, 3–14.
40 R. Golestanian, T. B. Liverpool and A. Ajdari, *Phys. Rev. Lett.*, 2005, **94**, 220801.
41 J. R. Howse, R. A. L. Jones, A. J. Ryan, T. Gough, R. Vafabakhsh and R. Golestanian, *Phys. Rev. Lett.*, 2007, **99**, 48102.
42 G. Rückner and R. Kapral, *Phys. Rev. Lett.*, 2007, **98**, 150603.
43 J. L. Anderson, *Annu. Rev. Fluid Mech.*, 1989, **21**, 61–99.

44 W. F. Paxton, K. C. Kistler, C. C. Olmeda, A. Sen, S. K. S. Angelo, Y. Cao, T. E. Mallouk, P. E. Lammert and V. H. Crespi, *J. Am. Chem. Soc.*, 2004, **126**, 13424–13431.
45 J. A. Theriot, T. J. Mitchison, L. G. Tilney and D. A. Portnoy, *Nature*, 1992, **357**, 257–260.
46 G. A. Smith, D. A. Portnoy and J. A. Theriot, *Mol. Microbiol.*, 1995, **17**, 945–951.
47 E. D. Daniel Blair. *The Matlab Particle Tracking Code Repository.* http://physics.georgetown.edu/matlab/index.html.
48 J. Crocker, *J. Colloid Interface Sci.*, 1996, **179**, 298–310.